Measure of the chaotic domain in simple Hamiltonian systems

Carles Simó

Dept. Matemàtica Aplicada i Anàlisi, UB, Barcelona, Catalunya

carles@maia.ub.es

Hamiltonian Perturbation Theory: Separatrix Splitting, Theory and Applications

Centro di Ricerca Matematica Ennio De Giorgi

Pisa, 5 to 9 May 2014

Dedicated to the memory of Michel Hénon (1931–2013), a pioneer introducing paradigmatic models.

The problem

Many phenomena are described using a **Hamiltonian formulation**. **Integrable cases** can be useful approximations.

There are methods to detect the **lack of integrability**: either **algebraic** or **analyic** or based on **numerical evidences**.

A key point: **which is the amount of chaos in a given system?**

If small (below some threshold) perhaps it can be **neglected for practical applications**.

If it is large **perhaps it takes so long to show up that one exceeds the time of validity of the model**.

Some crucial questions

- **Which are the dynamical objects responsible for the chaos?**
- **Can they be detected and measured in some reasonable way, to be able to predict the amount of chaos of the system?**
- **How do the answers to these questions depend on the level of energy and on the parameters of the system?**

Some theoretical background

We consider **analytical** Hamiltonian systems. The simplest ones are the **integrable systems**. Assume $H(q,p)$ is a Hamiltonian with n degrees of freedom: $(q,p) \in U \subset \mathbb{R}^{2n}$ or $(q,p) \in \mathbb{T}^n \times V, V \subset \mathbb{R}^n$.

Integrability is considered in the **Liouville-Arnold** sense:

- There exist n **first integrals** $F_1, \ldots, F_n, \{H, F_j\} = 0$,
- They are in **involution**: $\{F_i, F_j\} = 0$,
- **Functionally independent** almost everywhere.

We recall that if the **level $F^{-1}(c)$ is compact** then it is $\simeq \mathbb{T}^n$ (Arnold).

How to detect non-integrability?

A typical method is to derive **necessary conditions for integrability**. It they are not satisfied we have **obstructions to integrability**.

For simplicity we denote the Hamiltonian equations as $\dot{z} = X^H(z)$.

Necessary conditions

Let $z(t)$ a solution. Here $t \in \mathcal{D} \subset \mathbb{C}$**, a complex domain**. The image of $\mathcal{D}$ under z is a **Riemann surface** $\mathcal{R}$. Let $\gamma(t)$ be a **closed path in** $\mathcal{R}$.

Along $\gamma(t)$ we consider the **first order variational equations VE1**: $\frac{dA}{dt} = DX^H(z(t)A$.

The entries of $DX^H(z(t)$ belong to some **field of meromorphic functions** K but the ones of A belong to **some extension** L.

This leads to consider the **Galois group** G_1 **of the extension**. It is an **algebraic group**. Then the following results follows

Theorem (Morales-Ramis). If H is integrable with meromorphic first integrals in a neighborhood of $\mathcal{R}$, then the identity component $(G_1)^0$ is abelian.

A classical theorem by Ziglin follows as a Corollary.

If **VE1 gives no obstructions** (i.e.: $(G_1)^0$ is abelian) one can pass to **higher order variational equations VEm**.

Note that VEm are non-linear. But they can be **reduced to a linear system by introducing additional variables**.

As before the entries of the coefficient matrix belong to some field K and the entries of the solution to an extension L.

One can introduce the corresponding **Galois group G_m**. Then

Theorem (Morales-Ramis-S.). If H is integrable with meromorphic first integrals in a neighborhood of $\mathcal{R}$, then the identity component $(G_m)^0$ must be abelian for all m.

There exist **symbolic algorithms** and **numerical ones, made rigorous by CAP** to test for obstructions.

Standing problem: **the above methods are very useful to detect non-integrability** but without **quantitative information** (at least up to now).

KAM theory

Let H_0 integrable with $F^{-1}(c)$ compact. One can introduce **angle-action variables** $(\varphi, I) \in \mathbb{T}^n \times V$, $V \subset \mathbb{R}^n$ and H_0 can be written as $H_0(I)$.

Solution: I =ctant, $\varphi(t) = \varphi(0) + t\omega(I)$, where $\omega(I) = \nabla(H_0(I))$ is the frequency vector. $\mathbb{T}^n \times V$ is foliated by **invariant tori** with n-frequencies quasiperiodic motion if $\omega(I)$ is **non-resonant**: $(k, \omega(I)) \neq 0 \; \forall k \in \mathbb{Z}^n \setminus \{0\}$.

Do the tori subsist under perturbation? That is, for $H(\varphi, I, \varepsilon) = H_0(I) + \varepsilon H_1(\varphi, I, \varepsilon)$.

Theorem (KAM). The tori subsist, with a small deformation, provided

- The frequencies satisfy a **Diophantine condition**:

$$|(k, \omega)| \geq c/|k|^\tau \quad \text{for all} \quad k \in \mathbb{Z}^n \setminus \{0\}, \quad \text{for some} \quad c > 0, \tau > 0,$$

- H_0 satisfies a **non-degeneracy condition**: $\mathrm{Hess}(H_0(I))$ must be a regular matrix. This is called the torsion condition.
- The parameter ε must be **sufficiently small**.

Measure of the complement of KAM tori: $\mathcal{O}(\varepsilon^{1/2})$.
Similar results for **symplectic maps**.

Measuring the amount of chaos

There are different tools, mainly based on **frequency analysis** and on estimates of the **maximal Lyapunov exponent** or some variants.

In **frequency analysis** one tries to check if an orbit can be assumed to be **quasiperiodic** for $t \in [0, T_1]$, to obtain a **basis of the frequencies** and to check if it is preserved for $t \in [T_2, T_3], T_2 > T_1$.

For **Lyapunov estimates**, let x_0, v_0 be an initial point and a random unitary vector. Compute the **Lyapunov sums** $LS_k, k>0, LS_0=0$ using

$$w_k = DF(x_{k-1})v_{k-1}, \;\; v_k = \frac{w_k}{||w_k||_2}, \;\; LS_k = LS_{k-1} + \log(||w_k||_2), \;\; x_k = F(x_{k-1}).$$

The **maximal Lyapunov exponent** Λ, if it exists, is the **limit slope** of LS_k as a function of k.

There exist **algorithms (like MEGNO) to speed up the convergence** and, more useful for the study we want to do, to decide if $\Lambda > 0$ **(chaotic dynamics)** or $\Lambda = 0$ **(regular dynamics, generically)**.

In both cases one should select **suitable methods to sample** in the levels of energy.

The examples to be considered

We consider several **simple Hamiltonian systems**, around a **positive definite totally elliptic** point, either **resonant or non-resonant** with **two and three degrees of freedom**. The compact levels of energy are diffeomorphic to $\mathbb{S}^3$ or to $\mathbb{S}^5$.

- The **classical HH** case: $H = \frac{1}{2}(x^2 + y^2 + p_x^2 + p_y^2) + x^3/3 - xy^2$,
- A **variant of the HH** case: $H_0 = \frac{1}{2}(x^2 + y^2 + p_x^2 + p_y^2) - xy^2$,
  Emphasis and details about the **role of separatrix maps**,
- A **non-resonant** case: $H_{nr} = \frac{1}{2}(x^2 + y^2 + p_x^2 + 2p_y^2) + xy^2$,
  Depending on time we can also consider
- A **three-degrees of freedom in 1:1:1 resonance** family:
  $$H_{3r} = \frac{1}{2}(x^2 + y^2 + z^2 + p_x^2 + p_y^2 + p_z^2) + Ax^2y + By^2z + Cz^2x.$$
- A **three-degrees of freedom non-resonant** case:
  $$H_{3nr} = \frac{1}{2}(x^2 + y^2 + z^2 + p_x^2 + 2p_y^2 + 3p_z^2) + x^2y + y^2z + z^2x.$$

Next we provide **results** and **theory supported explanations** .

The classical Hénon-Heiles Hamiltonian

Poincaré section: $y=0, \dot{y}>0, h=0.1$. Note the **3 hpo and manifolds**.

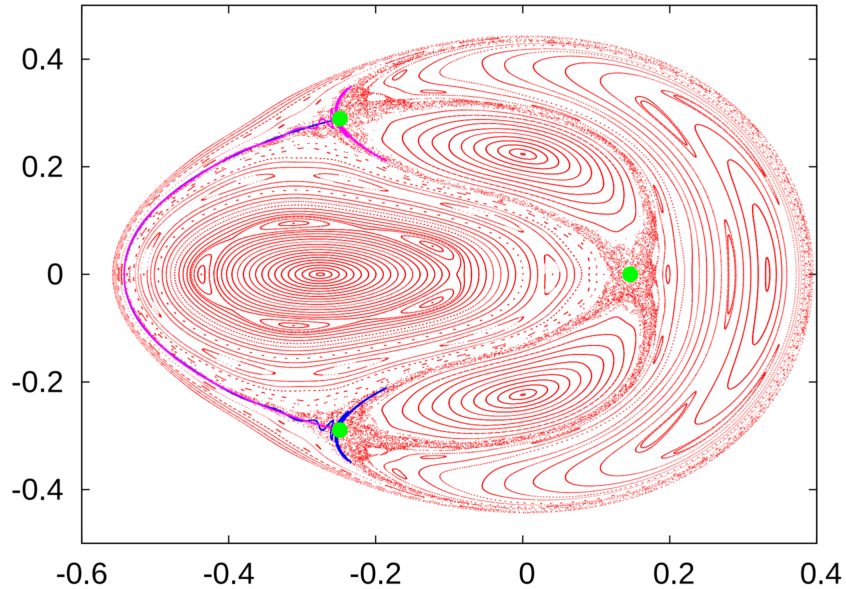

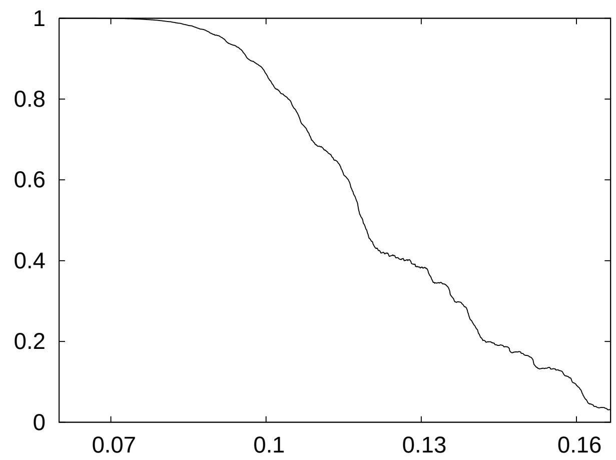

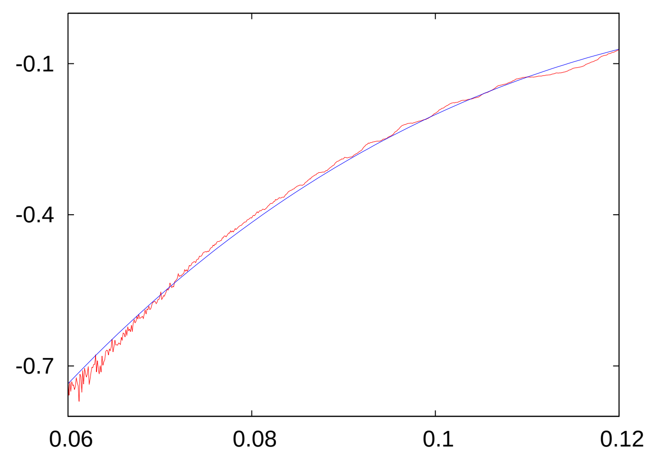

Left: **regular fraction** $\psi(h)$ **vs** h; right: $h\log(1-\psi(h))$ **vs** h and a fit by $a_c h + b_c h\log(h) - c_c$. Note $h \leq 1/6$ for compact levels.

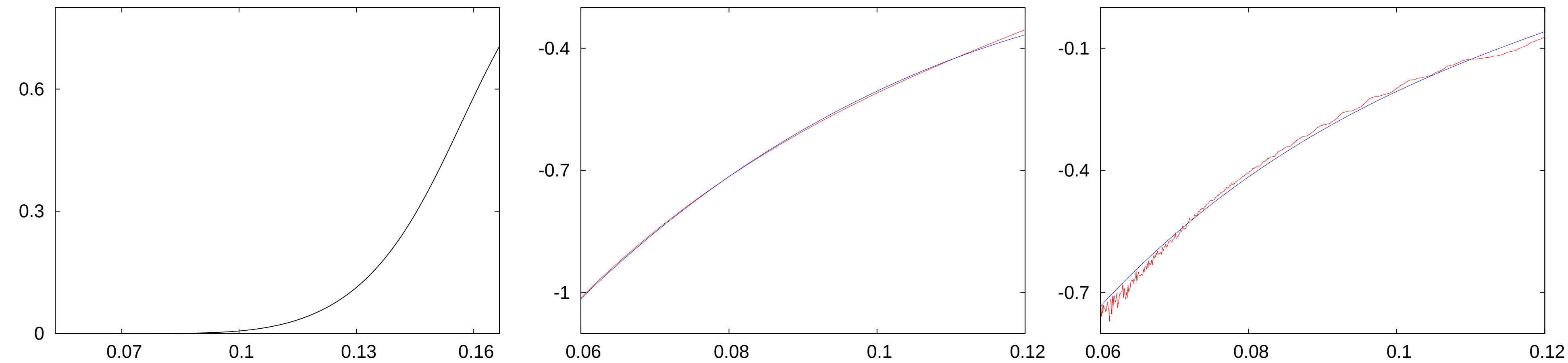

Left: **splitting angle $\sigma(h)$ of $W^{s,u}$ from fixed points of the Poincaré map**, measured on $y = 0, x < 0$, vs h.
Middle: $h\log(\sigma(h))$, excluding values of h for which $\sigma(h)$ is **too small** to be confident on the dp values, and large values of h, for which the **destruction of invariant curves around period 5 orbits plays an additional role**. We also plot (in blue) a **fit** $a_s h + b_s h \log(h) - c_s$.
Right: Comparison of $h\log(1-\psi(h))$ and a multiple of **the $\sigma(h)$ fit**. Same value of $c : c_c = c_s$. Changes in a and $b : b_c = b_s - 1$ (following from an analysis of the **separatrix map**).

There is a nice relation between the measure of the chaotic set and the splitting of the manifolds of the periodic hyperbolic orbits. As can be expected now (not in 1962!), this is exponentially small.

Additional background

The **scaling** $x = \nu X,\ y = \nu Y,\ p_x = \nu P_X,\ p_y = \nu P_Y$ and $h = \nu^2/2$ leads to have ν **in front of the cubic terms** in H. If $h \to 0$ the Poincaré map **tends to the identity**.

The usual **suspension and averaging** lead to approximate the Poincaré map by an autonomous **Hamiltonian, integrable,** vector field plus errors **with bounds exponentially small in** ν. A little change (previous passage to **NF to order 4**) replaces ν by ν^2.

If $F_\varepsilon : z \mapsto z + \varepsilon F(z)$ is a **near the Id 2D symplectic map** and the limit flow (suitably normalized) has a **separatrix** $\beta(t)$ s.t. is analytical for $|\mathbf{Im}(t)| < \rho$, then

Theorem (Fontich-S). For a given small fixed value η the **splitting** $\mu(\varepsilon)$ of the manifolds for F_ε has **a bound**

$$\mu(\varepsilon) < A \exp\left(-\frac{2\pi(\rho - \eta)}{\zeta(\varepsilon)}\right),$$

where $\zeta(\varepsilon) = \log(\lambda(\varepsilon))$ and $\lambda(\varepsilon) =$ **maximal eigenvalue** at the hyperbolic fixed point of F_ε.

In fact, for singularities **located at** $\pm\rho\mathrm{i}$ generic estimates have the form

$$A\varepsilon^{B}\exp(-2\pi\rho/\zeta(\varepsilon))(1+o(1)),$$

while singularities **located at** $\pm\rho\mathrm{i}\ \pm\delta$ give

$$A\varepsilon^{B}\exp(-2\pi\rho/\zeta(\varepsilon))(\cos(2\pi\delta/\zeta(\varepsilon)+\varphi(\varepsilon))+o(1)).$$

When the cos term is close to zero we can expect to **see the effect of next harmonic**, which adds

$$A_2\varepsilon^{B_2}\exp(-4\pi\rho/\zeta(\varepsilon))\cos(4\pi\delta/\zeta(\varepsilon)+\varphi_2(\varepsilon)).$$

More complicated patterns show up if there are singularities at $\pm\rho\mathrm{i}\pm\delta_j$, $j=1,2,\ldots,k$ for which, beyond the exponentially small term, the **splitting can be quasiperiodic in** $1/\zeta(\varepsilon)$.

We also note that, due to some symmetry, it can happen that the **dominant terms in the splitting are not associated to the closest singularities to the real axis**.

Not just the splitting is relevant, but the **relative position of** W^u **wrt** W^s.

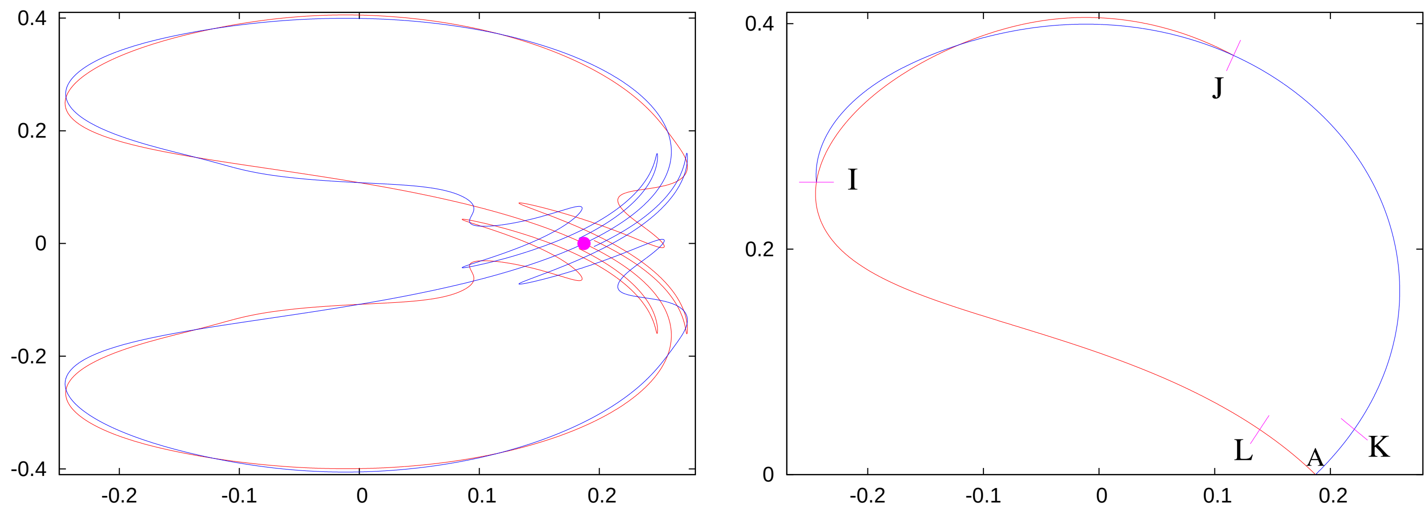

The **separatrix map** gives the return to a strip (around $W^{u,s}$ between the sections I, J in the plot) after **passing close to A**. In the **simplest, symmetrical, formulation** can be approximated by

$$SepM : \begin{pmatrix} \xi \\ \eta \end{pmatrix} \to \begin{pmatrix} \bar{\xi} = \xi + c - \log(|\bar{\eta}|)/\zeta \pmod{2\pi} \\ \bar{\eta} = \eta + \mu \sin(\xi) \end{pmatrix}.$$

In turn, it can be approximated for $\eta \geq \mu/\zeta$, by the **standard map**

$$SM_\kappa : \begin{pmatrix} u \\ v \end{pmatrix} \to \begin{pmatrix} \bar{u} = u + \bar{v} \\ \bar{v} = v + \kappa \sin(u) \end{pmatrix}.$$

For $\kappa > \kappa_G \approx 0.971635406$ **(Greene's value)** has dynamics which is **mostly chaotic**, explaining the **quantitative results for HH system**.

A variant of the HH case

Poincaré section: $y = 0, \dot{y} > 0, h = 0.1$. Note the **hpo and manifolds**.

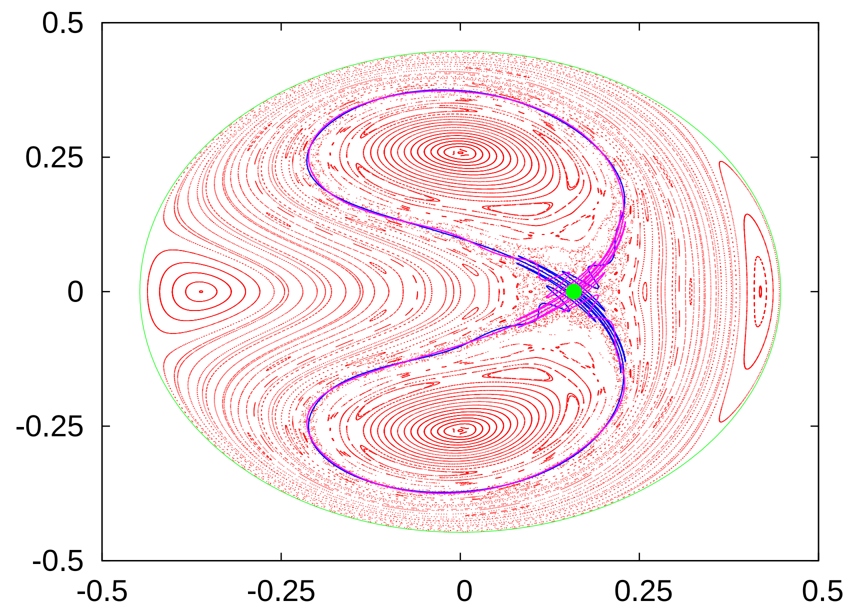

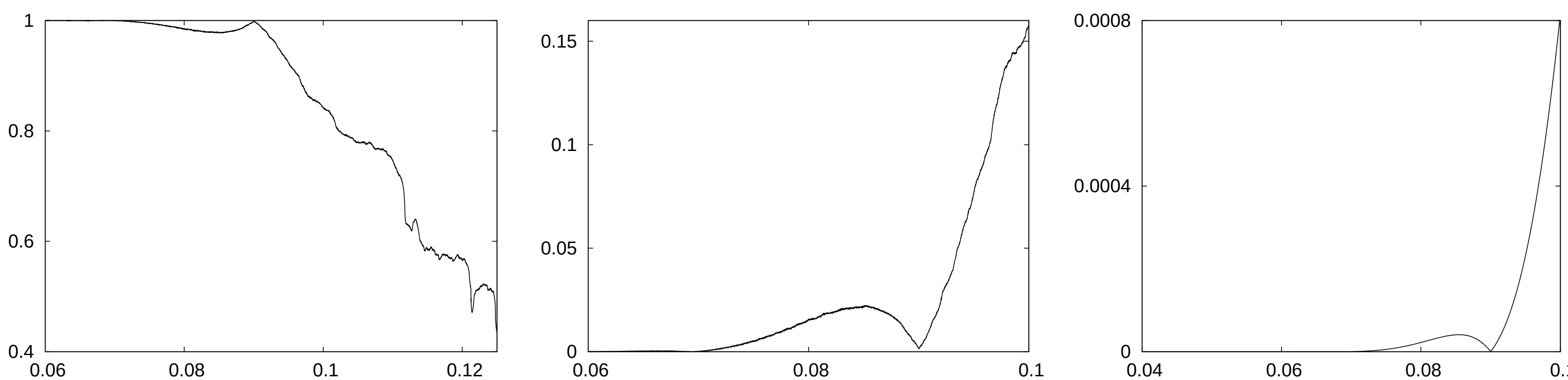

Left: $\psi(h)$ vs h. Middle $1 - \psi(h)$ vs h. Right: the **splitting $\sigma(h)$ of the manifolds** as seen in the top plot. **Why $1 - \psi(h)$ and $\sigma(h)$ are not uniformly tending to zero when $h \to 0$?** $(h \leq 1/8)$.

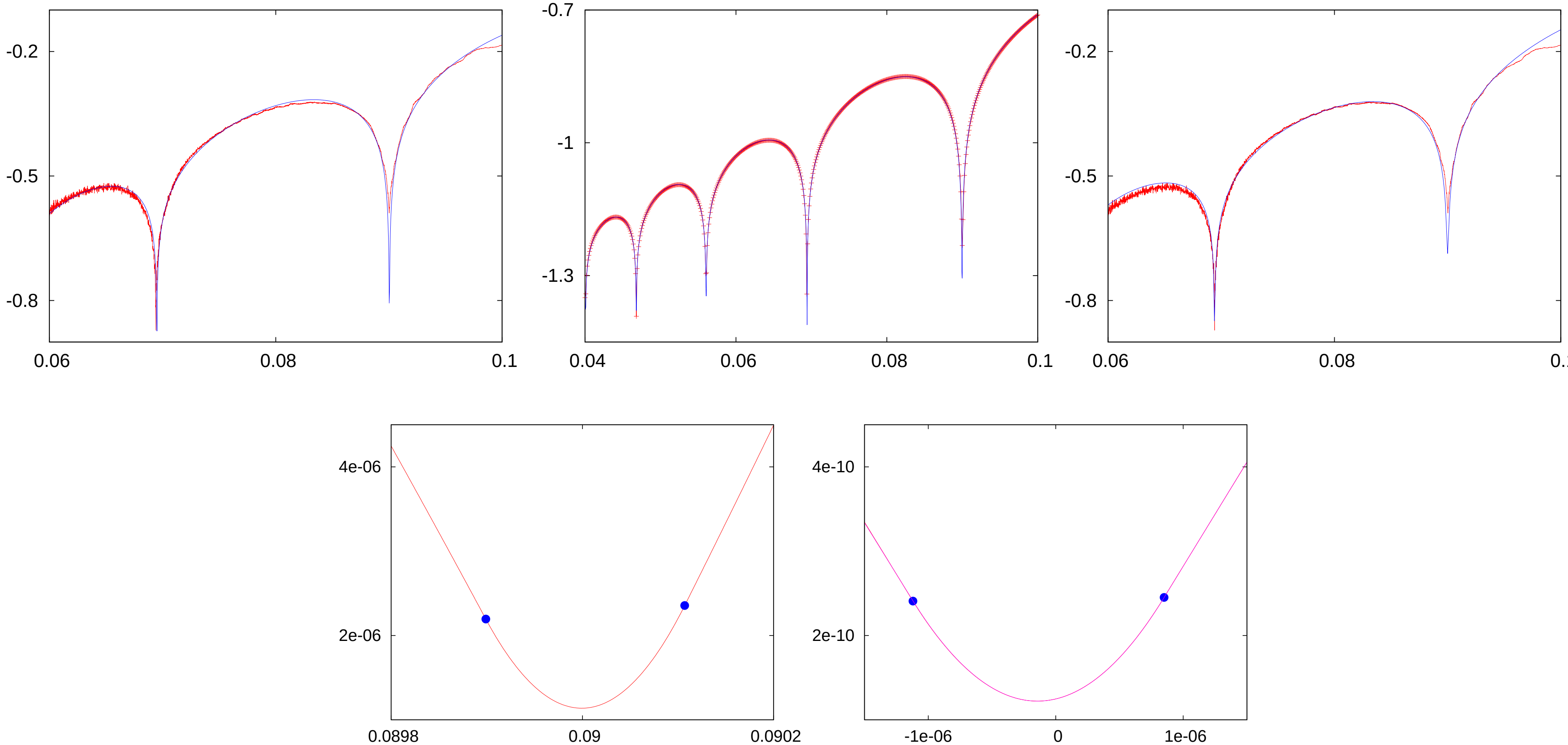

Remark: In the present case we do not measure $\sigma(h)$ as an angle but **as the sum of the (absolute values of the) areas of lobes**.
Top row: Left: $h\log(1-\psi(h))$ and a fit (not as usual!). Middle: $h\log(\sigma(h))$ and related fit. Right: $h\log(1-\psi(h))$ and a multiple of the fit for $\sigma(h)$, as in the HH case. Lower row: Left: A magnification of the **behaviour of $\sigma(h)$ near the rightmost minimum** $h \approx 0.089999$. Right: Similar for **next minimum** $h \approx 0.06941635$ and a fit to a theoretically derived formula.

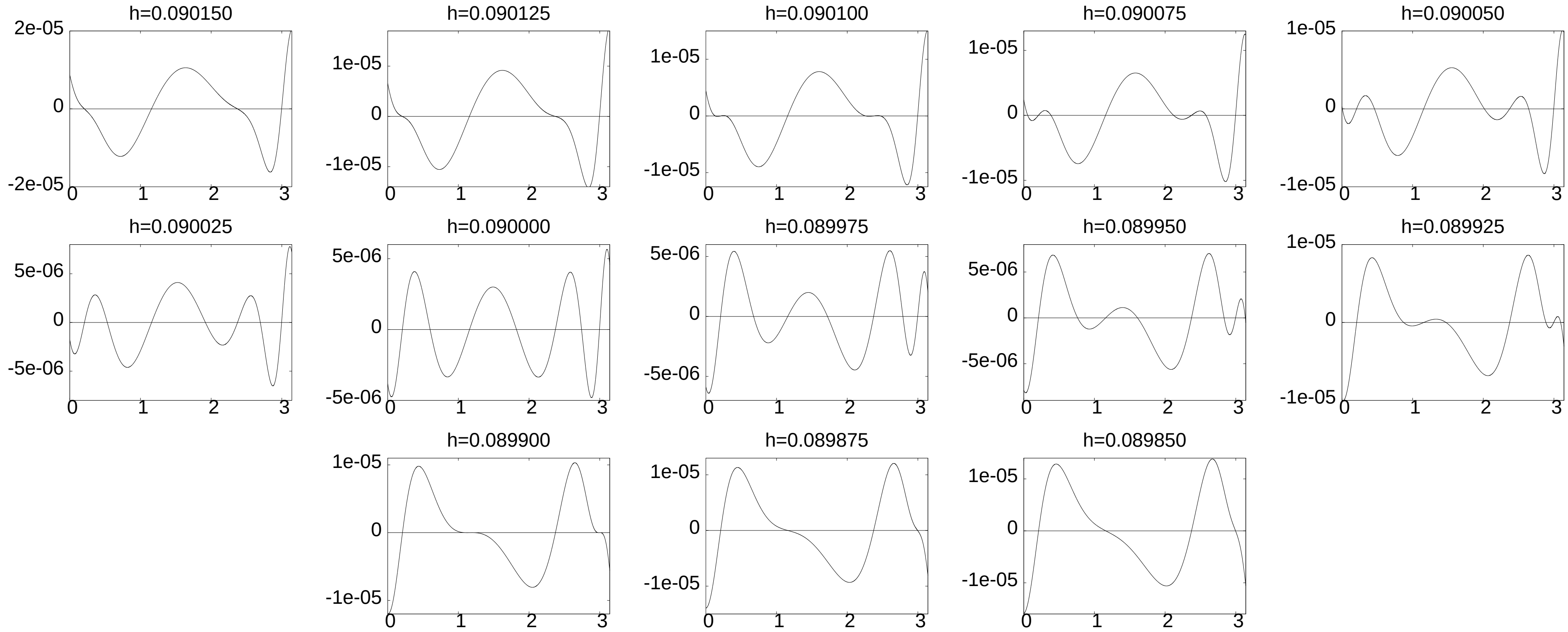

A **movie of the position of W^u wrt W^s as a function of h** around the rightmost minimum. It shows **cubic tangencies and new homoc.**

Why?: The oscillation of W^u wrt W^s is periodic (in suitable variables), but now the **first harmonic has a factor like** $\cos(2\pi\delta/\zeta(h) + \varphi(h))$, which becomes zero for some h. The **second harmonic plays a role**.

In the **related standard map** $\sin(x)$ is replaced by $\cos(2\pi\alpha)\sin(x) + \sin(2\pi\alpha)\sin(2x)$, with $\alpha \in (-\pi/2, \pi/2]$ as **additional parameter**.

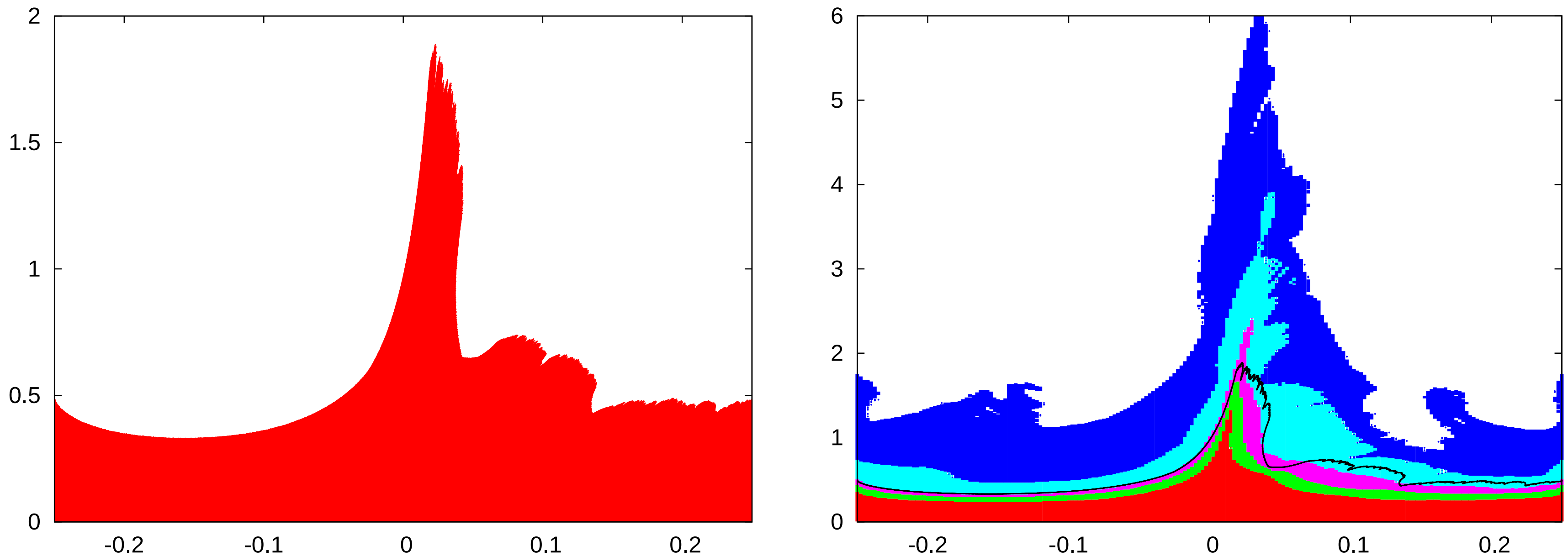

Left: Range of values (α, ε) (ε denotes now the previous κ) for the **two-harmonics standard map** $SM_{\varepsilon,\alpha}$ for which **there exist rotational invariant curves**.

Right: From lower to upper part **domains with regular fraction exceeding 0.9, 0.7, 0.5, 0.3, 0.1**. For comparison, the boundary of the left plot shown in black.

With some different factors this **relates the splitting measures to the abundance of chaotic motion**. Note that for the **critical values** the amounts of regular and chaotic dynamics **are similar**.

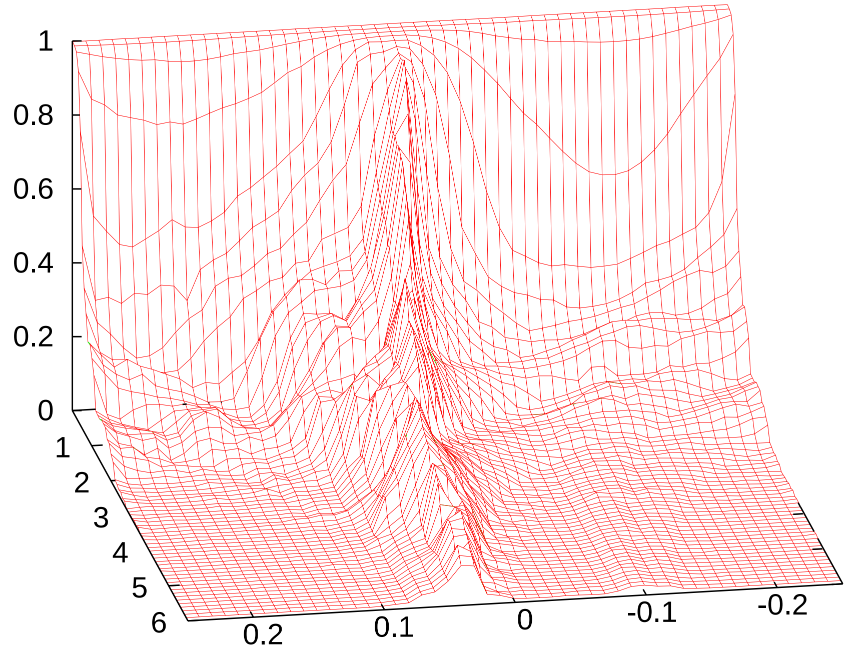

A 3D view of the **fraction of regularity** $\psi(\alpha, \varepsilon)$.

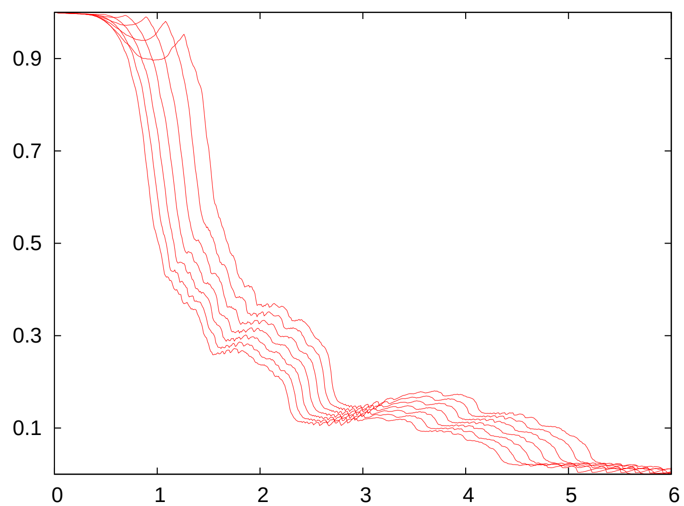

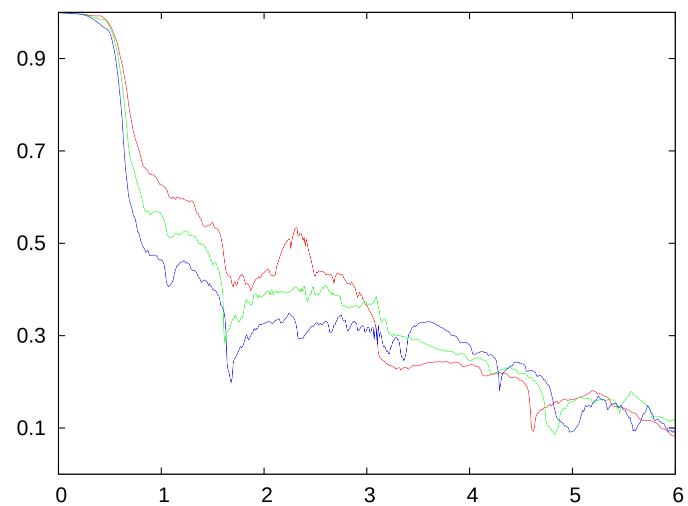

Curves $\psi(\alpha, \varepsilon)$. Left: $\alpha = k/400, k = 0, ..., 6$. Rigth: $100\alpha = 3, 3.5, 4$. **Singularities** of the limit flow separatrix: $\pm i\,\pi/2 \pm \log(\sqrt{1+\Delta} + \sqrt{\Delta}), \Delta = 2\tan(2\pi\alpha)$.

Details on the two-harmonic standard map

$\mathrm{SM}_{\varepsilon,\alpha}(x,y) \to (\bar{x} = x + \bar{y}, \bar{y} = y + \varepsilon(\cos(2\pi\alpha)\sin(x) + \sin(2\pi\alpha)\sin(2x)))$.
The change $(\alpha, x) \leftrightarrow (1/2 - \alpha, x + \pi)$ **preserves the map**. But for some illustrations it is advisable to consider the **full range** of α. E.g. to see the different behavior for $x = 0$ and $x = \pi$.

Fixed points on $(0,0), (\pi,0)$ and on $(0, \cos^{-1}(-1/(2\tan(2\pi\alpha)))$.

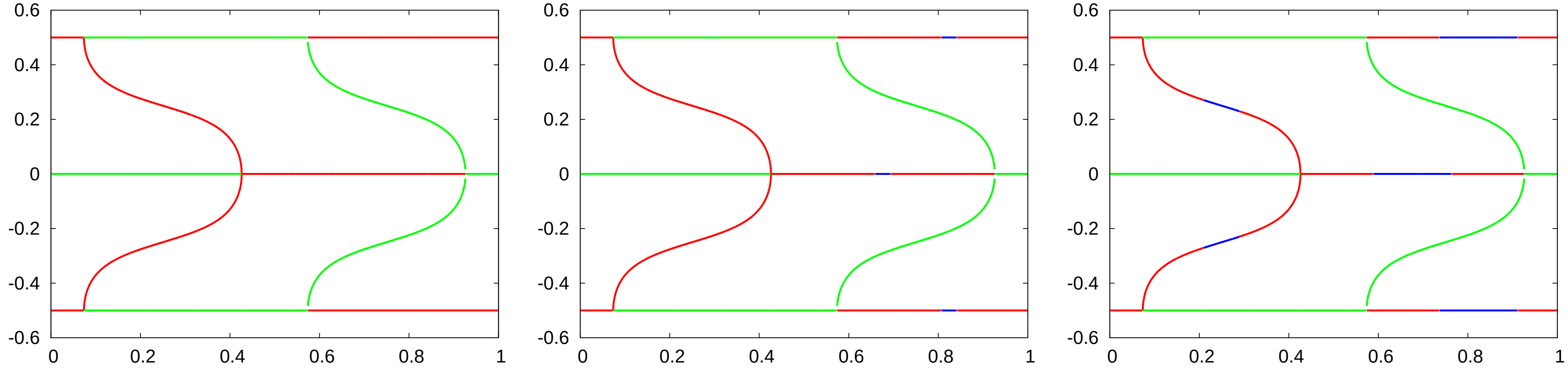

Location of the **fixed points** in $(\alpha, x/(2\pi))$ variables for $\varepsilon = 1.0, 1.8, 2.1$ from left to right. Color code: Red for **elliptic E**, green for **hyperbolic H**, blue for **hyperbolic with reflection HR**.
Bifurcations from $x = 0, \pi$ for $\alpha_0 = \tan^{-1}(1/2)$ and for $1/2 - \alpha_0, 1/2 + \alpha_0, 1 - \alpha_0$ (for all ε). **Creation of HR** for $\varepsilon = 4/\sqrt{5}$ and $\varepsilon = 2$.
The behaviour of the **period 2 orbit** at $(0,\pi), (\pi,\pi)$ is shown in the plot.

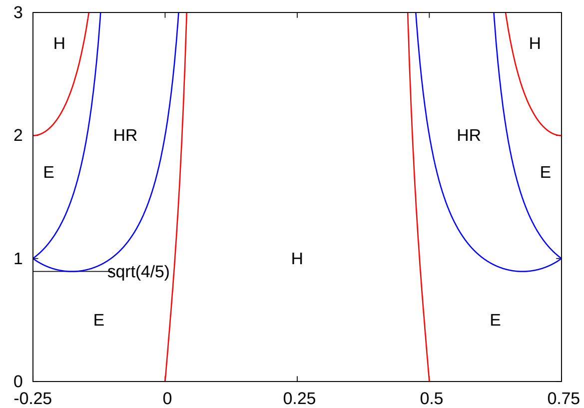

Other **period 2 orbits** behave and bifurcate in a richer way. Shown in next **movie** where (α, x) is displayed for several ε.

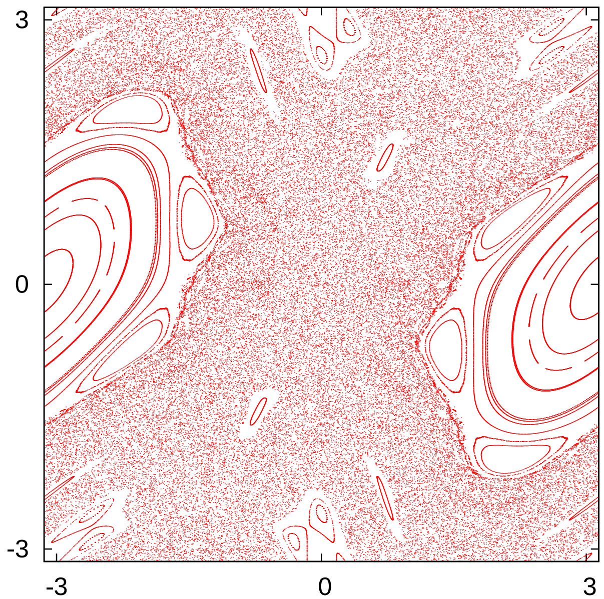

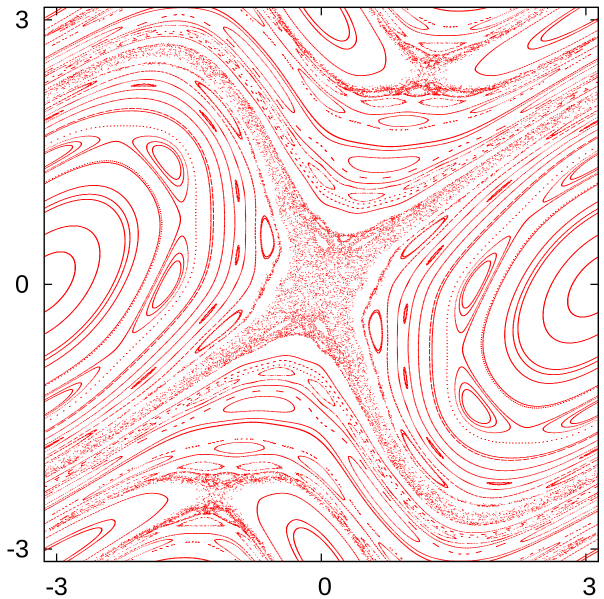

Phase portrait for $\varepsilon = 1.5$. Left: $\alpha = 0$. Right: $\alpha = 0.02$.
Next **three movies** illustrate changes and **the reasons why they occur** for different (α, ε).

A 2 dof non-resonant case

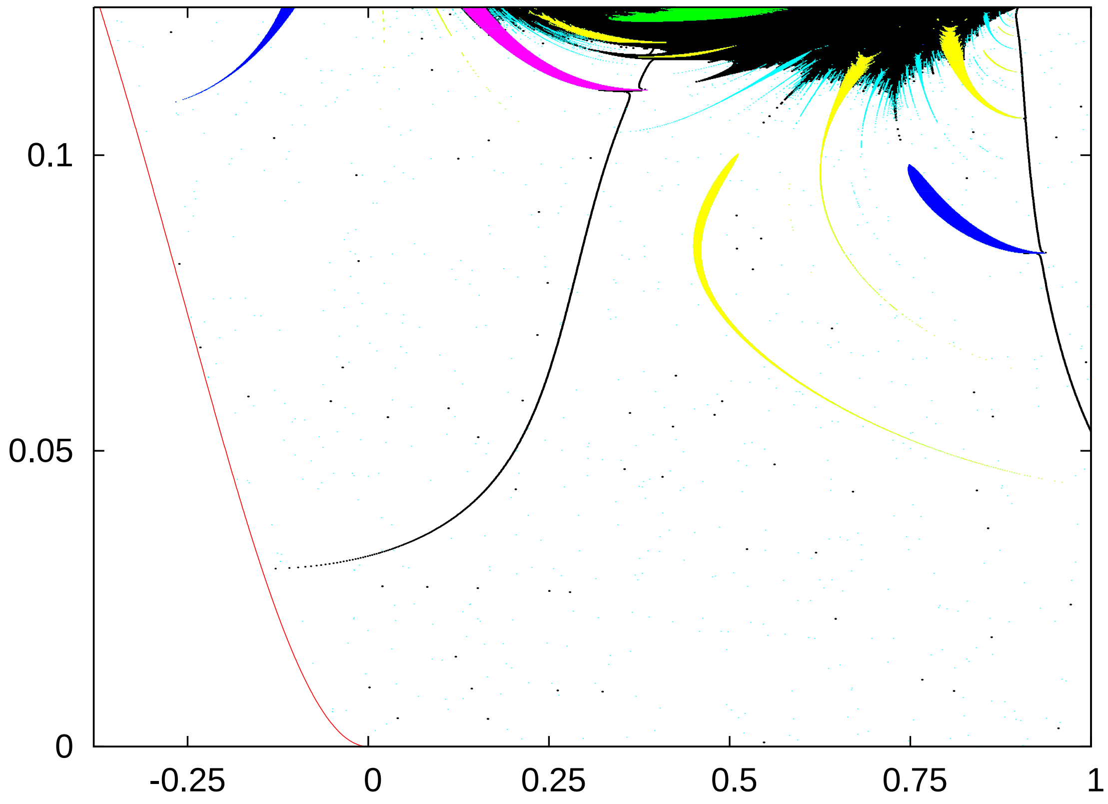

Information based on rotation number ρ: Scaled variables, $h \leq 1/8$, initial points on $y = 0, p_x = 0, p_y > 0$.
Red curve: p.o. Black curves: non-twist (max at left, min at right). Black domain: chaos. Green, blue, magenta: periods 3, $\rho = 1/4$, $\rho = 2/7$. Yellow: periods between 9 and 19, mainly dominated by the p.o. with $\rho = 3/11, 3/13, 5/19$ and $3/10$. Higher periods marked in light blue.

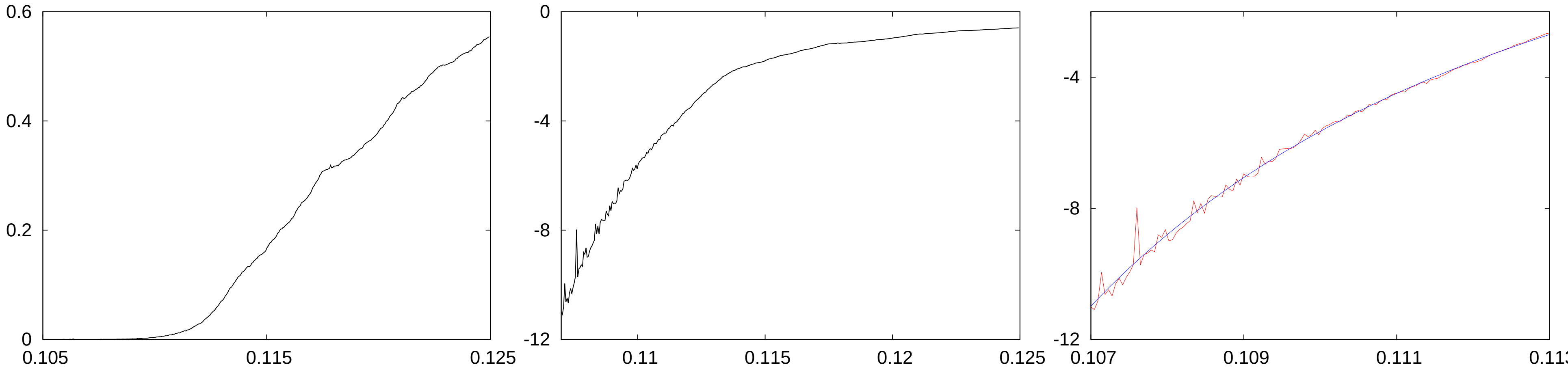

Left: the values of $1-\psi(h)$ vs h. Middle: Same plot using log scale for $1-\psi(h)$. Right: A part of previous plot and an **adapted fit**.

The fit used: $\log(1-\psi(h)) = a + b\log(h-h_c) - \frac{c}{(h-h_c)^d}$.

Best fit: $h_c = 0.09850650$ **with** $d = 1$.

The h_c value coincides with the **passage of the period-4 p.o. from elliptic to hyperbolic**. That is: the upper tip of the right blue region in previous figure.

Based on **normal form to order 4**, assuming **Diophantine condition** at the fixed point, **resonances** of order $|k|_1$ require $h > \hat{c}/|k|_1^{1+\tau}$. Reciprocally: $|k|_1 = \mathcal{O}(h^{-1/(1+\tau)})$ with **amplitude** $\mathcal{O}(\exp(-\rho|k|_1))$, where ρ is now the **analyticity width** after producing NF_4. This implies **doubly exponentially small** bounds in the amount of chaos.

A three-degrees of freedom family in 1:1:1 resonance

It can be seen as a **generalisation of HH to 3 dof**; allows to **study the 1:1:1 resonance**; allows to **break all symmetries** if $A \leq B \leq C$ with $<$ in all cases. Clearly, we can normalise $A+B+C=3$. It contains some **degenerate cases**.

Problem 1: we cannot expect $\psi(h) \to 1$ as $h \to 0$. The normal form, truncated to order 4 NF_4 has only, in general, H_2 and NF_4 as first integrals. **One can not expect integrability of the NF**.
This **lack of integrability** has been easily checked for all A, B, C using Morales-Ramis theorem.

Problem 2: As for $h \to 0$ the system approaches a harmonic oscillator, **any Poincaré map tends to the identity**. To distinguish regular from chaotic via Lyapunov exponents **is computationally expensive**.
Sketch of the solution to this problem: 1) scale variables by $\varepsilon = \sqrt{h}$; 2) compute NF in (I, φ); it is enough to order 4; 3) introduce slow angles $\alpha_j = \varphi_j - t$; 4) average the equations wrt t; 5) scale time by h; 6) let $h \to 0$.

We obtain an **homogeneous quartic Hamiltonian H_4**.

$$
\begin{aligned}
&4H_4(u,v,w,p_u,p_v,p_w) = \\
&\quad A^2(-5u^4+(-20v^2-10p_u^2+4p_v^2)u^2-48uvp_up_v-5p_u^4+(4v^2-20p_v^2)p_u^2) \\
&+B^2(-5v^4+(-20w^2-10p_v^2+4p_w^2)v^2-48vwp_vp_w-5p_v^4+(4w^2-20p_w^2)p_v^2) \\
&+C^2(-5w^4+(-20u^2-10p_w^2+4p_u^2)w^2-48wup_wp_u-5p_w^4+(4u^2-20p_u^2)p_w^2) \\
&+AB((-20vw-28p_vp_w)u^2+8(vp_w+wp_v)up_u+(-28vw-20p_vp_w)p_u^2) \\
&+BC((-20wu-28p_wp_u)v^2+8(wp_u+up_w)vp_v+(-28wu-20p_wp_u)p_v^2) \\
&+CA((-20uv-28p_up_v)w^2+8(up_v+vp_u)wp_w+(-28uv-20p_up_v)p_w^2).
\end{aligned}
$$

Due to the scaling and passage to the limit, the **level of H_4 is irrelevant**.

One can easily compute the **limit value** $\lim_{h\to 0}\psi(h)$ of the regularity fraction from H_4.

For comparison, we show the **evolution of** $\psi(h)$, for a few of the sample of cases studied, using the initial Hamiltonian.

Furthermore we give evidence of the **numerical difficulties** to obtain consistent estimates of $\psi(h)$ for small h.

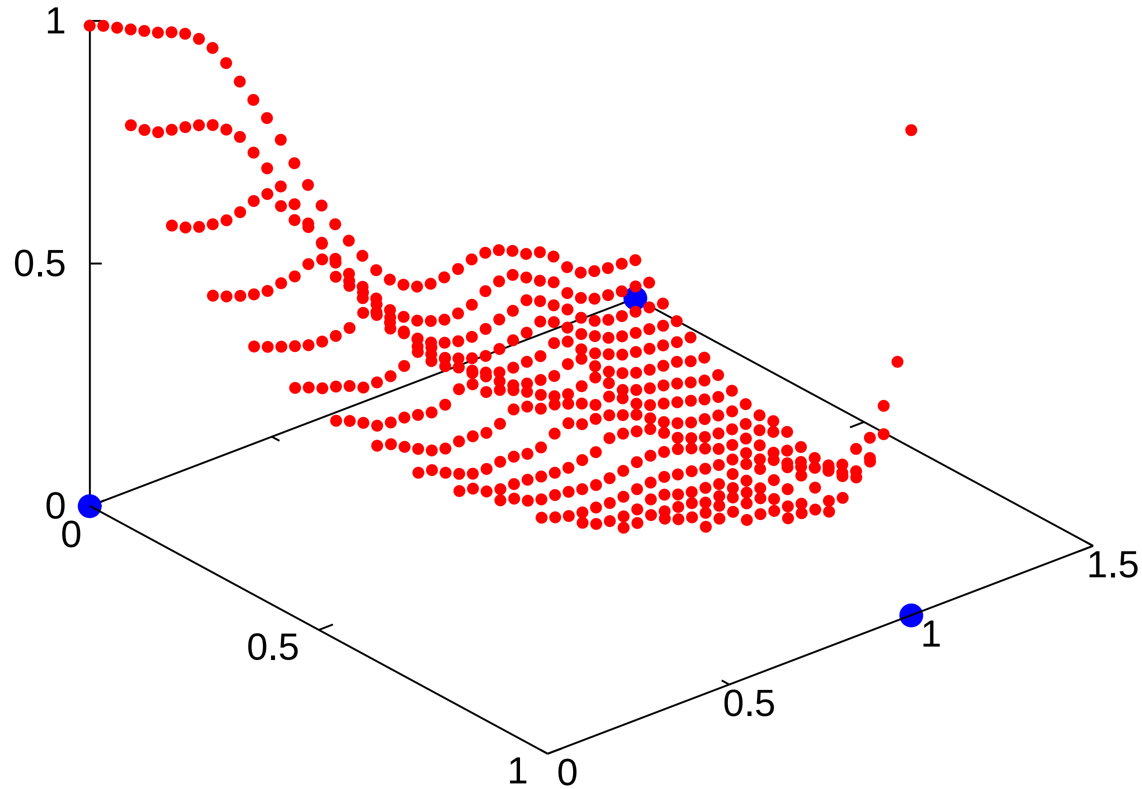

The **limit fraction of integrability** $\psi(0)$ as a function of $A \leq B \leq C$. The horizontal variables are A (ranging in $[0, 1]$) and B (ranging in $[0, 3/2]$). Then $C = 3 - A - B$.

The values of $\psi(0)$ are **away from 1** for most of the values of the parameters, except for the cases $(0, 0, 3)$ **and** $(1, 1, 1)$, to be discussed later.

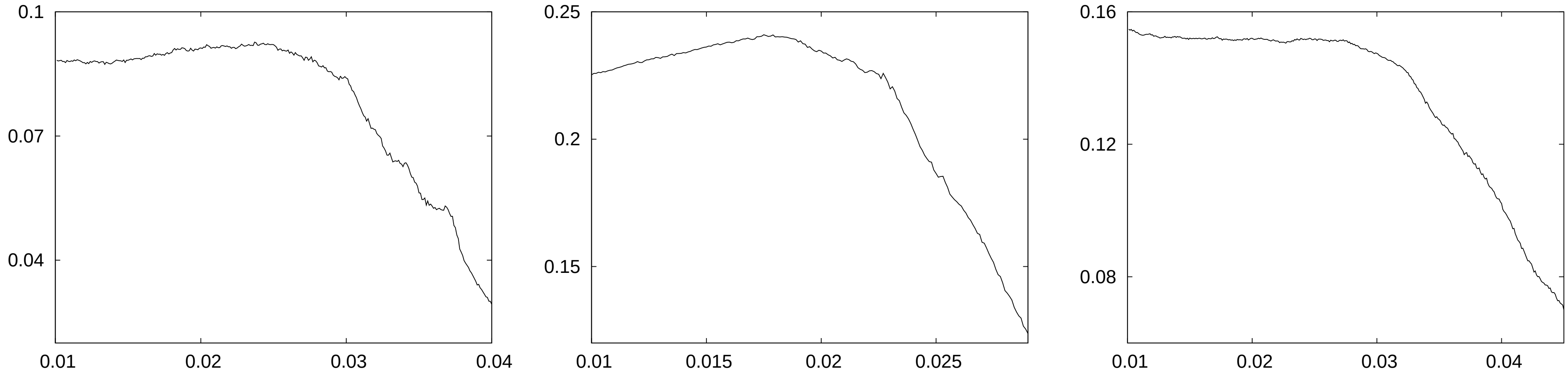

The **regular fraction** $\psi(h)$ as a function of the initial h for values (A, B, C) equal to $(0, 3/2, 3/2)$, $(0, 1, 2)$, $(1/2, 1, 3/2)$ is shown from left to right.

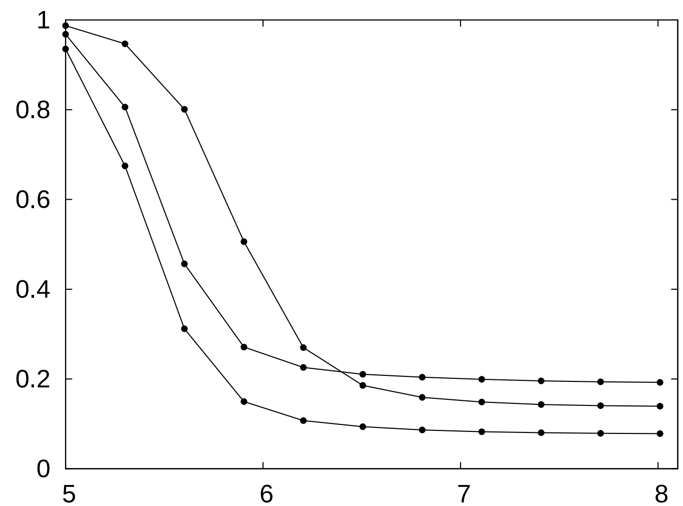

Estimates of $\psi(h)$ for $h = 10^{-4}$ as a function of the **maximal time** t_m used in the computations, shown in $\log_{10}$ scale. The limit values, from top to bottom, for the cases of previous figure from left to right.

From the dynamical measure ψ it seems that there are two cases $(A, B, C) = (0, 0, 3)$, $(A, B, C) = (1, 1, 1)$ **much more regular**. No **lack of regularity is detected using** H_4.

The case $(0, 0, 3), h \leq 1/72$, minimum for all A, B, C, could be expected. It coincides with the HH **variant model times an harmonic oscillator**. **What happens in the** $(1, 1, 1)$ **case ?** $h \leq 1/18$ (maximum).

From the **symmetry** one has that $u = x + y + z$ comes from the **1dof** $(u^2 + p_u^2)/2 + u^3/3$. Hence, it has **an extra integral**. The behaviour is similar to the 1:1 case. H_4 **that would detect only** $O(h)$ **chaos is unable to detect the exponentially small one**.

Surprisingly $1 - \psi$ for $(1, 1, 1)$ is **very small** (see plot) even for h close to $1/18$. It requires **large samples** to be confident on ψ.

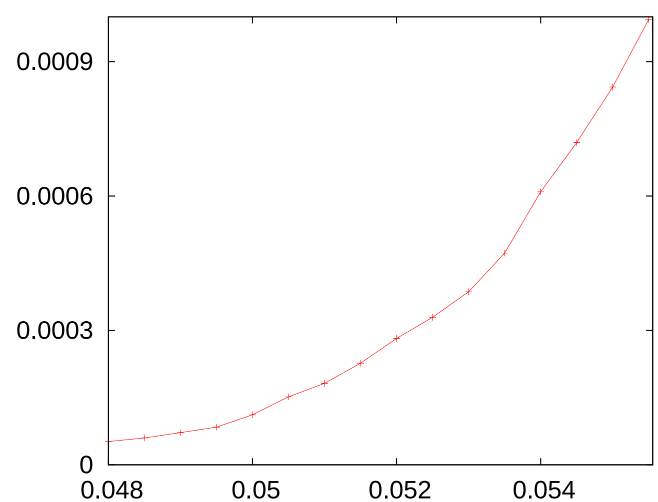

Some plots of the dynamics in the $(1, 1, 1)$ case in the section $x = 0$ which contains **3 fixed points p_j of the Poincaré map**. Energy: $h = 0.333^2/2$.

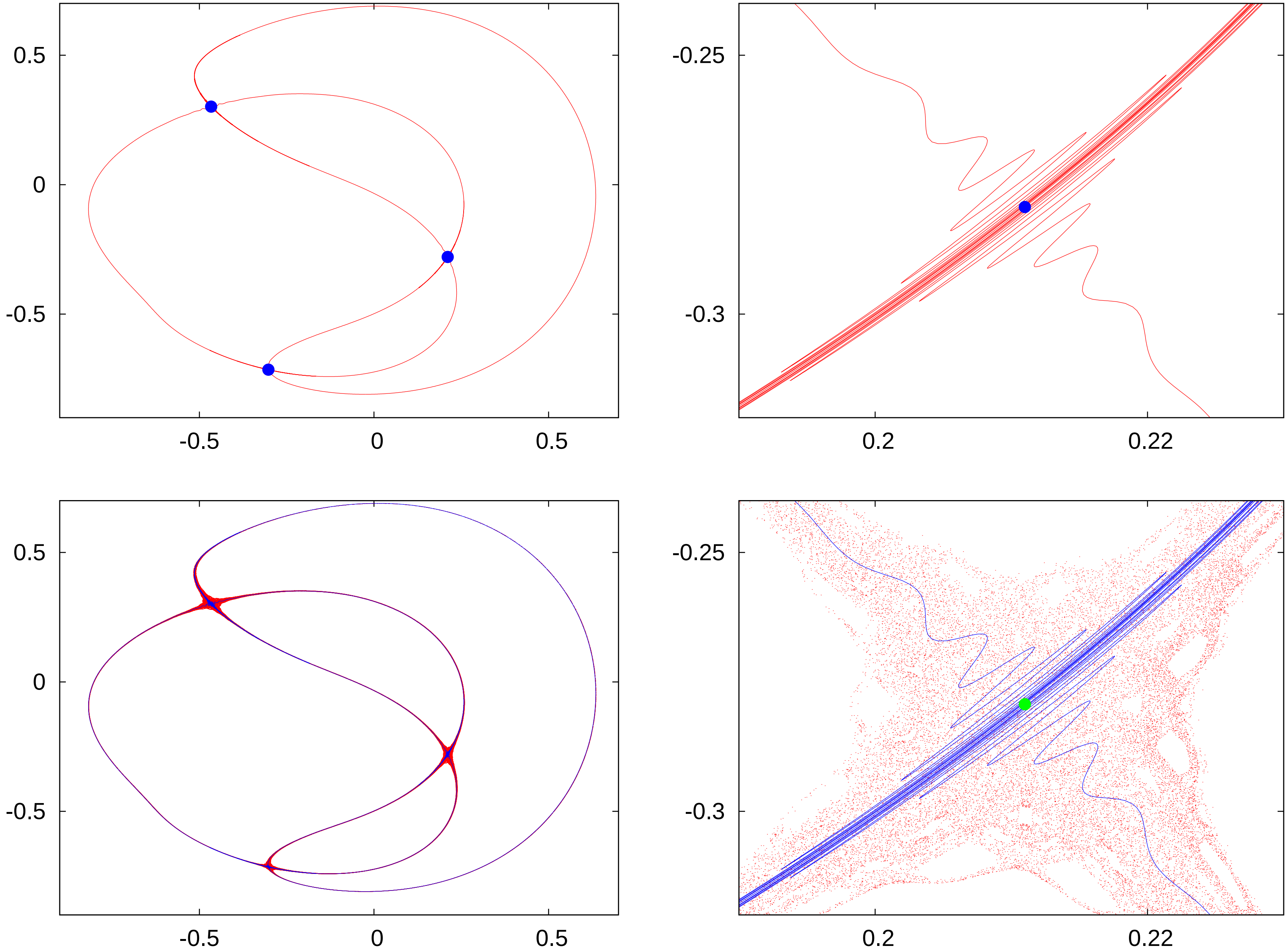

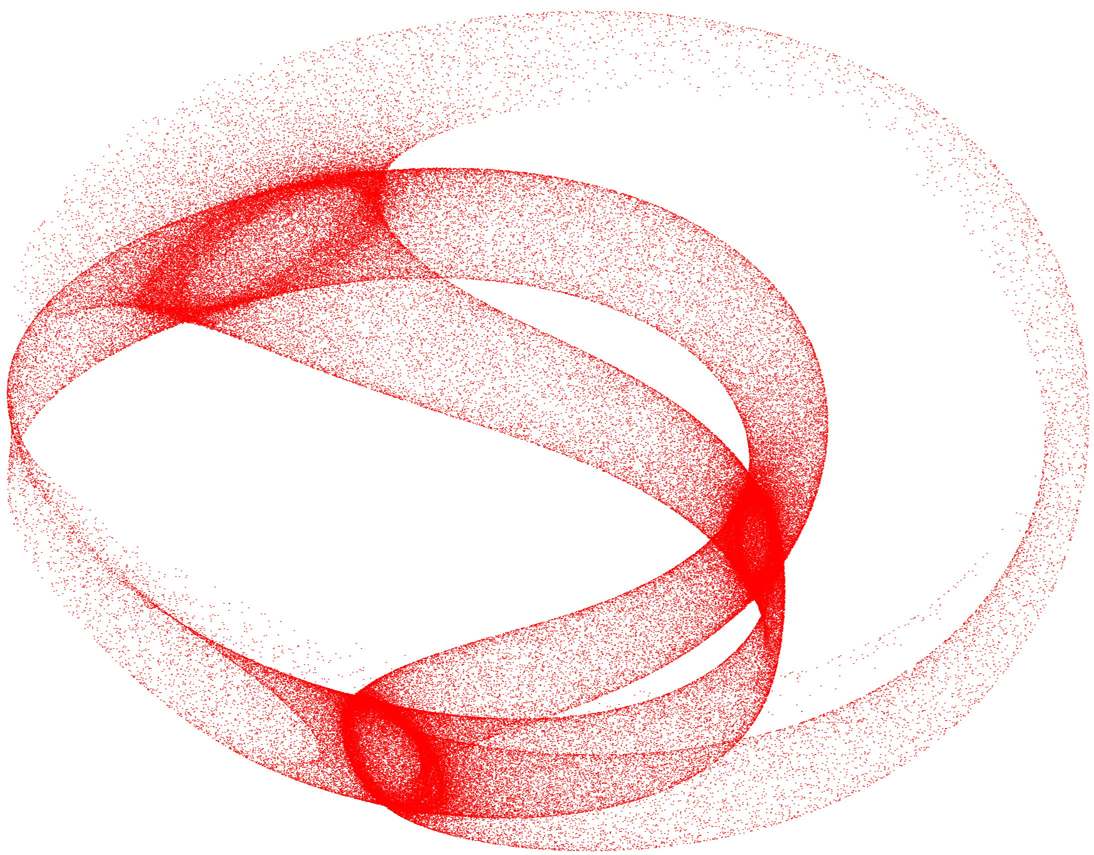

A 3D view of **iterates in $x = 0$, showing the heteroclinic chains between the $W^{u,s}$ of the centre manifolds of $p_j, j = 1, 2, 3$**.

Despite 10^9 **Poincaré iterates** have been computed (showing 1 every 5000) for an initial point, **close to an invariant curve** (in the Poincaré section) in one of the centre manifolds, and **heteroclinic connections occur**, the **amount of chaos is small**.

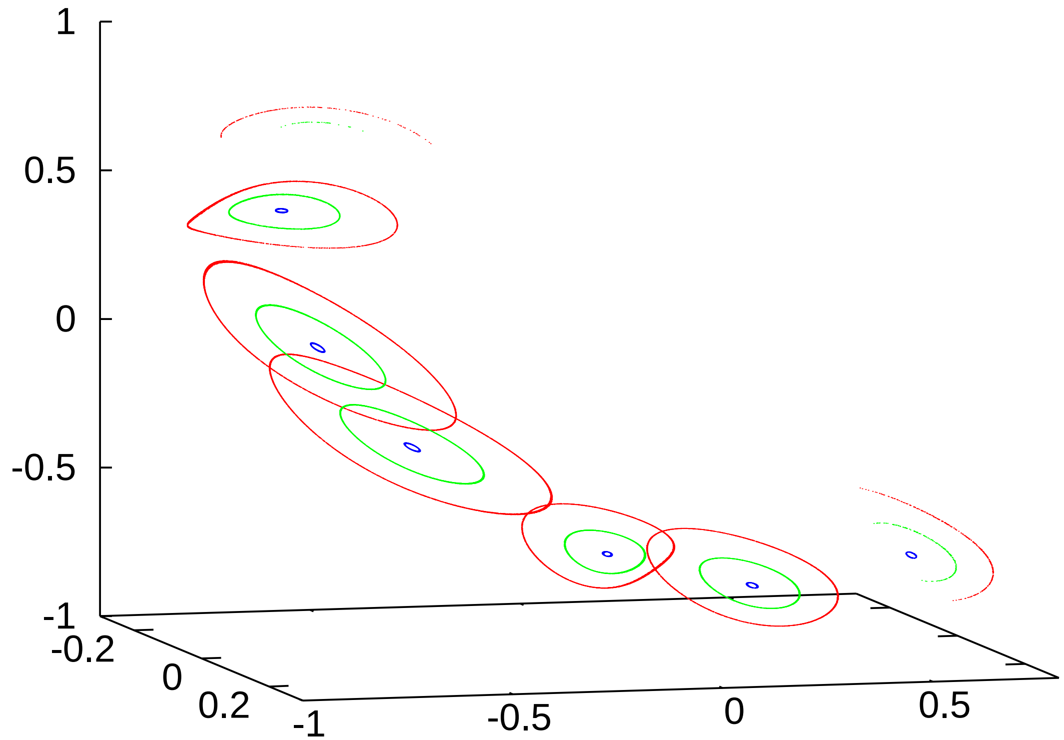

Slices of three cases using $|y| < 2.5 \times 10^{-5}$ like the one in previous figure for the **full set of 10^9 iterates**. Variables displayed $(z, \dot{y}, \dot{z})$ in $[-0.3, 0.3] \times [-1, .8] \times [-1, 1]$. One can see **six pieces** as expected. A piece is broken due to the fact that $x = 0$ is **not a global section**.

No **connections** between the three cases are seen: The **3D tori** in a level of energy **with an additional integral** prevent this.

A three-degrees of freedom non-resonant case

In present case the **frequencies at the fixed point are** $\omega = (1, \sqrt{2}, \sqrt{3})$. We should look for the location of **simple and double resonances** with the **Diophantine** and **simultaneous Diophantine** conditions

$$|(k,\omega)| \geq \frac{c_1}{|k|_1^{\tau_1}},\ \ \delta_m(\omega_2,\omega_3) = \min_{p\leq m}\{\min_{(q_2,q_3)\in\mathbb{Z}^2} |(q_2 - p\omega_2, q_3 - p\omega_3)|_\infty\},\ \ \delta_m \geq \frac{c_2}{|k|_1^{\tau_2}}.$$

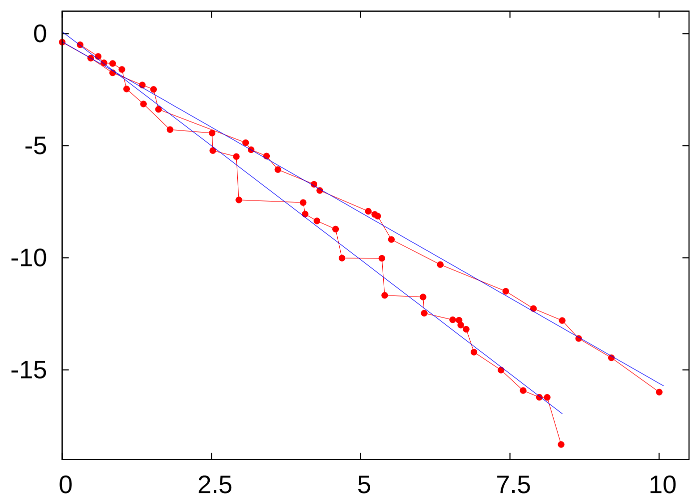

Values at which the **Diophantine bounds strictly decrease** as a function of $|k|_1$ or m (horizontal variable) and bound as vertical variable. Both in $\log_{10}$ scale. The linear fits have **slopes -2.035 and -1.524** for Diophantine and simultaneous Diophantine, respectively.

As in the non-resonant 2 dof case, the **amplitudes of simple and double resonances** have bounds
$\mathcal{O}(\exp(-c_1^* h^{-1/(1+\tau_1)}))$ and $\mathcal{O}(\exp(-c_2^* h^{-1/(1+\tau_2)}))$, for some positive c_1^*, c_2^*.
Hence, we should have a **very small amount of chaos for small energies**, showing local increase when resonances are created.

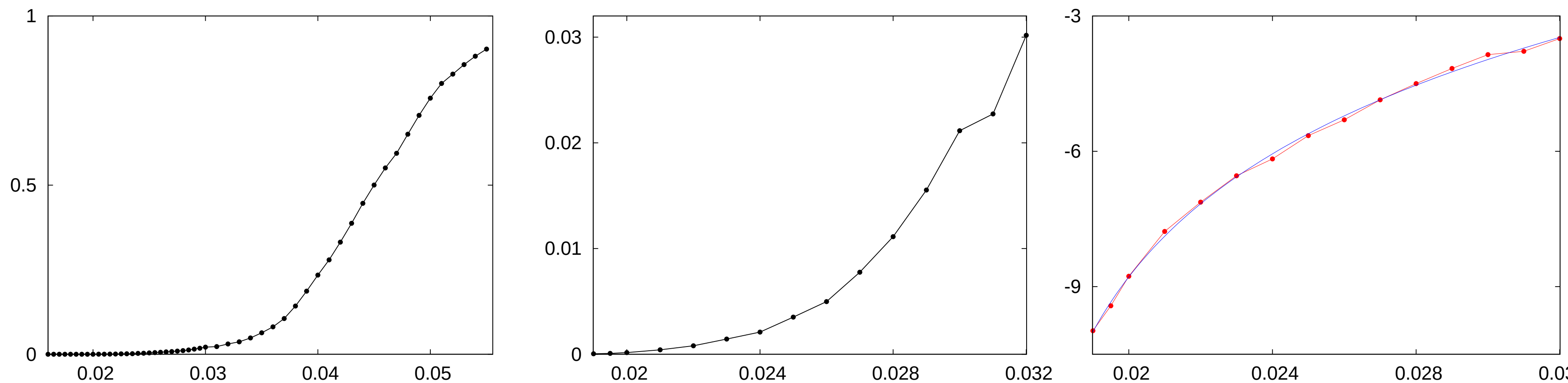

Left: Values of $1-\psi(h)$ **as a function of** h. Middle: A magnification on the interval $[0.019, 0.032]$. Right: On the same interval the values of $1-\psi(h)$ are shown in log scale and **a fit**.

The **fitting function** used for $\log(1-\psi(h))$ is not like the one used for non-resonant 2 dof, but of the form $\log(1-\psi(h)) = a + b\log(h-h_c)$.
The **exponentially small term is missing**. The best fit has been found for $h_c = 0.01656$. Reason: **most of the points in** $W^{u,s}(W^c)$ have **chaotic behaviour**.

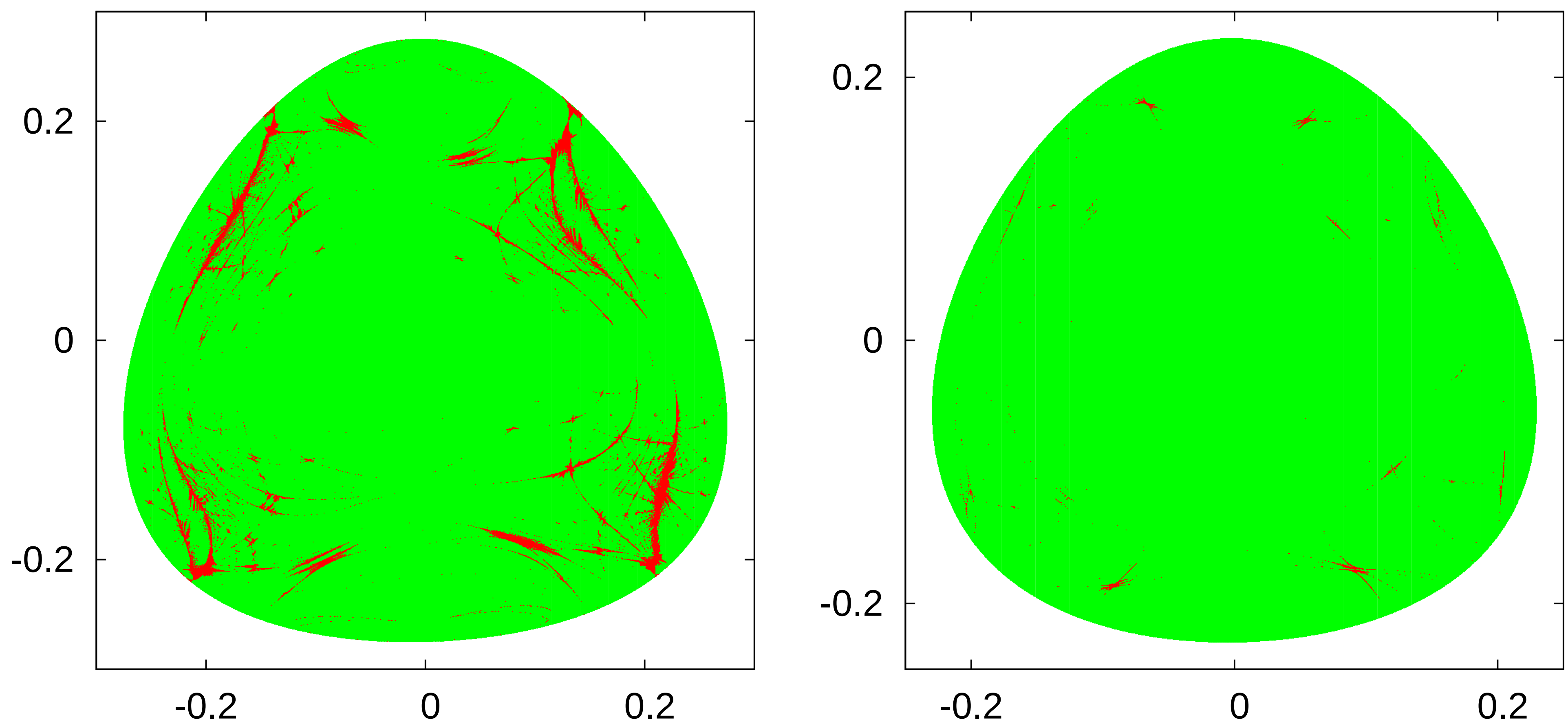

Location of the **chaotic zones** (in red) starting at a point of coordinates (x, y) with $p_x = p_y = p_z = 0$ and $z > 0$ derived from the energy. Left: for $h = 0.035$. Right: for $h = 0.025$.

For $h = 0.035$ one can see several **simple resonance channels** which cross at **double resonances**. For $h = 0.035$ only the location of **double resonance spots** and a small part of **tiny simple resonances** can be seen.

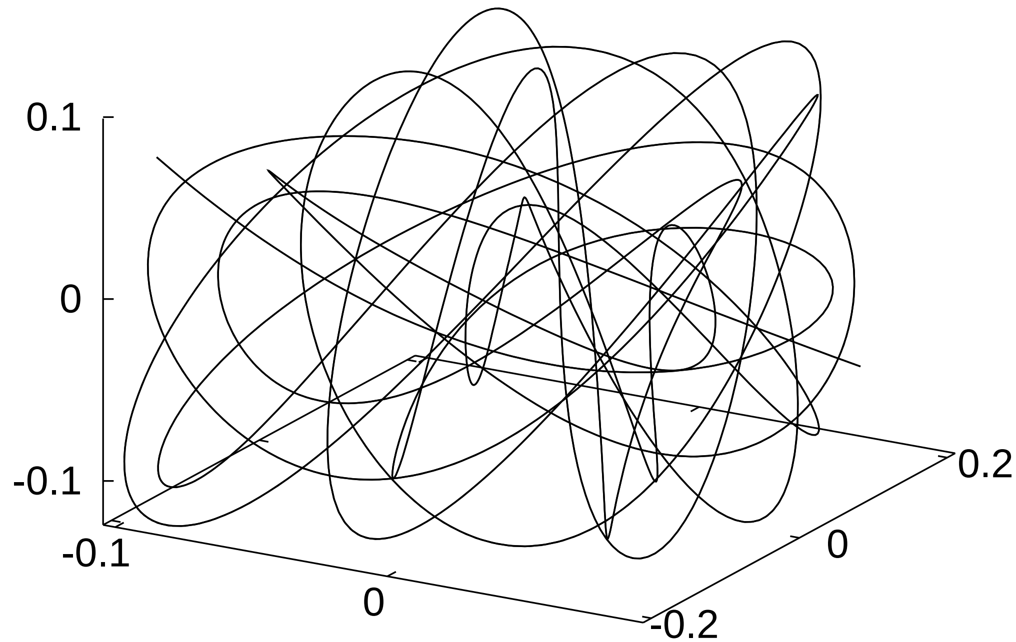

Near the middle of the **red spot close to** $x = -0.0916, y = -0.1864$ for $h = 0.025$ it is posible to find a **periodic orbit** of **elliptic-hyperbolic type**. We show a 3D view in (x, y, z).

Other **similar orbits emerge** from the other red spots.

They start to have these **stability properties** at a value of h which **can be identified as the h_c value in the fit**.

For this p.o. each one of the x, y, z variables **oscillates in a close to sinusoidal way**. Oscillations in one period, $T \approx 122.461344$: **19, 27 and 33**, resp. The **ratios** $27/19$ **and** $33/19$ are rather close to $\sqrt{2}$ and $\sqrt{3}$.

Motion in the 3D RTBP evolving from a vicinity of L_3

In contrast with the $(1, 1, 1)$ case of the 1:1:1 resonance, we show an example to **visualize diffusion and eventual escape**.

The L_3 **libration point** in the 3D RTBP is a **centre**$\times$**centre**$\times$**saddle**.

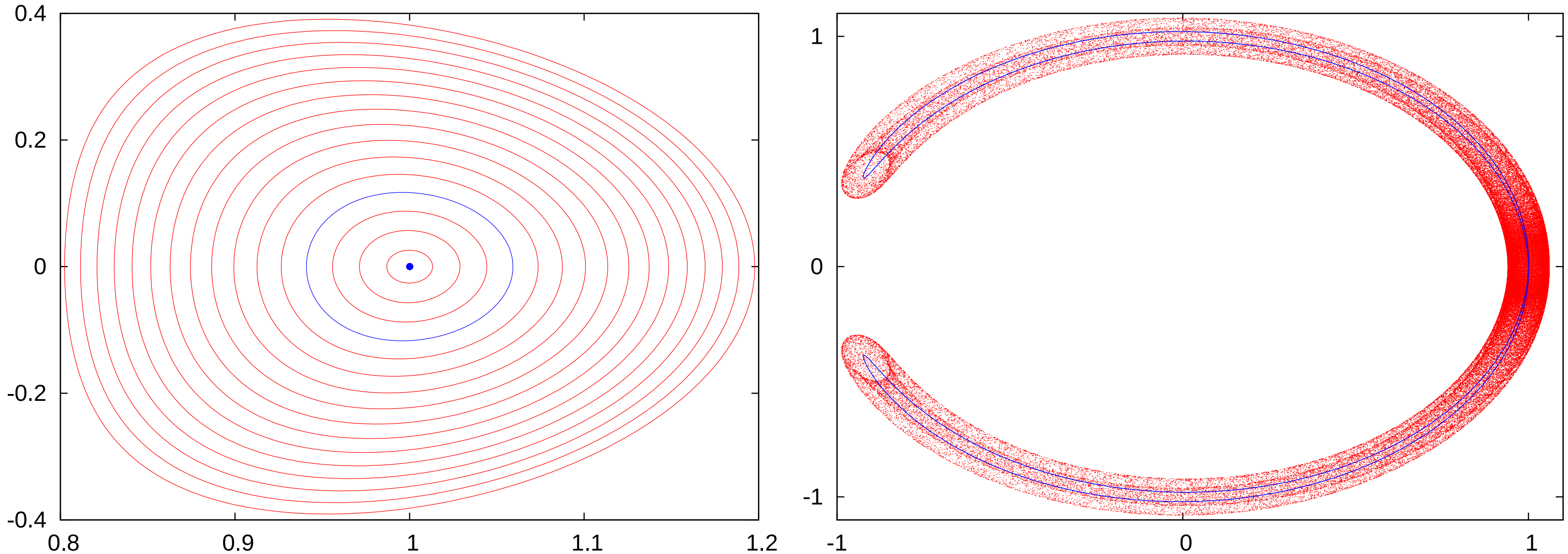

Left: **Invariant curves** on section $\Sigma = \{z = 0, \dot{z} > 0\}$ lying on $W^c(L_3)$ at the **Jacobi level** $C^* = 2.95998466228$ for **mass ratio** $\mu = 0.0002$. Right: Starting **close to the blue curve** in the left plot, the projections on (x, y) of the first 10^5 **Poincaré iterates** are shown. For reference a part of the **manifolds** of the **vertical Lyapunov p.o.** is displayed in blue.

Evidence of diffusion with **quasirandom passages near inv. curves**:
Left plot: **passages through a narrow 3D slice**, near $x = 0$ in Σ.
Green, blue and red points: passages after 10^5, 8×10^5 and 5×10^6 iterates.

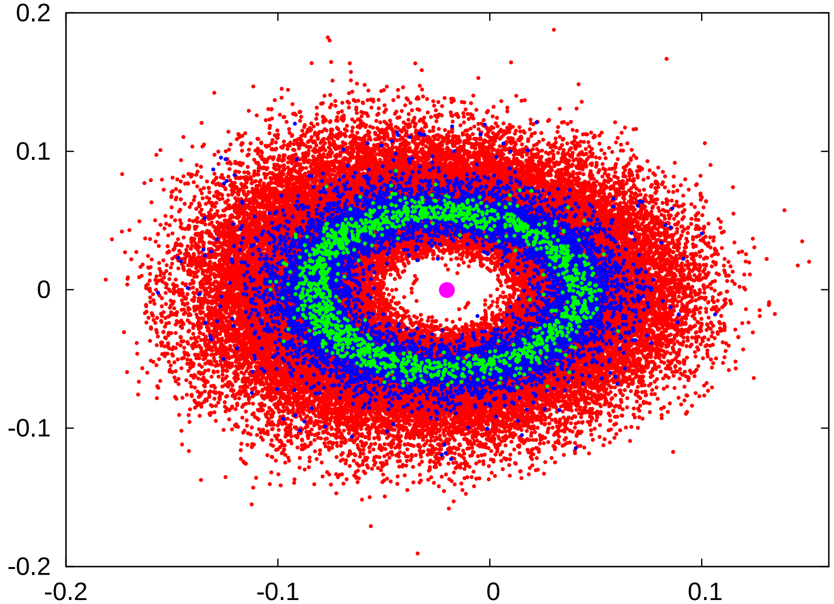

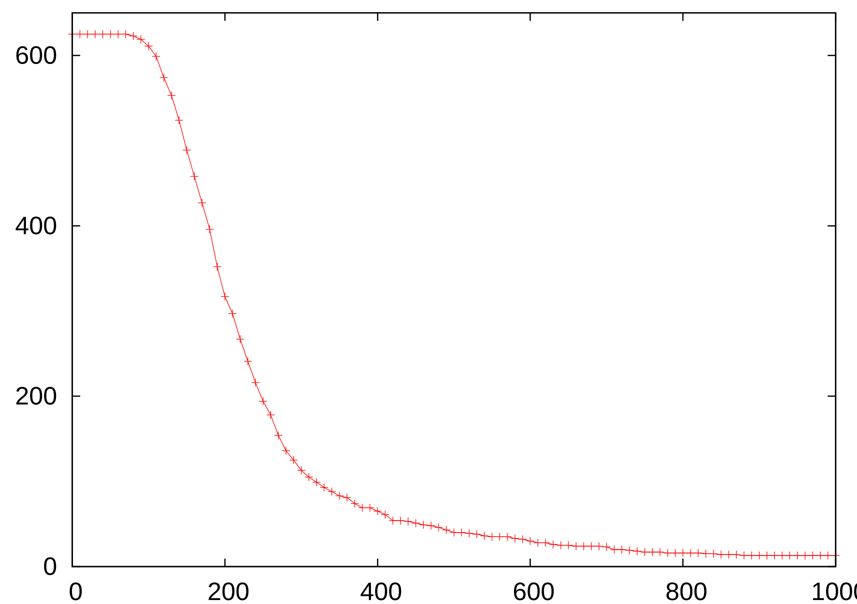

When the iterates are visiting points in $W^c(L_3)$ can approach the **horizontal Lyapunov p.o.** The manifolds of this one **come close to the secondary**. Some kind of **escape is produced**.

Right: Number of **non-escaping points as a function of the number of Poincaré iterates**. 1 unit $= 10^6$ iterates.

As expected: some of the initial points can **spend hundreds of millions of iterates** near a **sticky torus**.

Summarizing: **still an infinite amount of things to understand!**

But we are **guided by Michel Hénon insight in displaying key paradigmatic models**.

Understanding these models gives the basic ideas to understand many other phenomena.